Organic Electronics 87 (2020) 105937

Contents lists available at ScienceDirect

Organic Electronics

journal homepage: http://www.elsevier.com/locate/orgel

An ultra-thin inorganic interlayer strategy for achieving efficient inverted planar perovskite solar cells and modules with high fill factor

Ting Lei [a], Jie Xu [a], Jinbo Chen [a], Xinyi Zhu [a], Bo Jiao [a], Zhaoxin Wu [a,b,*]

[a] Key Laboratory for Physical Electronics and Devices of the Ministry of Education & Shaanxi Key Lab of Information Photonic Technique, School of Electronic and Information Engineering, Xi'an Jiaotong University, No. 28, Xianning West Road, Xi'an, 710049, China
[b] Collaborative Innovation Center of Extreme Optics, Shanxi University, Taiyuan, Shanxi Province, 030006, China

ARTICLE INFO

Keywords:
Perovskite solar cells
Vapor evaporation
Alkali metal fluorides
High fill factor
Stability

ABSTRACT

The fill factor (FF) is a fatal parameter to determine the power conversion efficiency (PCE) of perovskite solar cells. Especially, for the large area solar cells and modules, the low FF is the bottleneck towards the high PCE. The FF is highly correlated with the carrier recombination caused by defects at interfaces. Herein, we propose that ultra-thin inorganic alkali metal fluorides interlayer passivate the interface defects by vapor evaporation method at the perovskite/electron transport layer (ETL) interface. We confirmed that the alkali metal fluorides (AF) layer can function as both defect passivation layer and physical barrier layer, showing the significant enhancement of PCE and ambient stability. Eventually, we achieve the highest FF (80.6%) for 1 cm^2 size and highest FF (73.1%) for 10.8 cm^2 size perovskite solar cell by potassium fluoride (KF) as passivation layer. This functional interlayer strategy paves the way to resolve the industrial requirements with low cost, high fill factor large area planar perovskite solar cells.

1. Introduction

Organic–inorganic hybrid lead halide perovskite materials have attracted intense attention in the past few years owing to their superior photovoltaic properties [1–5]. To date, the power conversion efficiency (PCE) of perovskite solar cells (PSCs) with a solution-based route has rocketed to 25.2%, which is comparative with the efficiency of single crystal Si solar cells [6,7]. The reason why perovskite materials have excellent optoelectronic properties is structural fluctuations of soft octahedron $[PbI_6]^{4-}$ in perovskite crystals, which results in the correlated motion of charge carriers and the polar lattice forming large polarons [8–12]. The unique structural properties of perovskite materials lead to low carrier recombination rate beyond that of a simple direct band gap semiconductor [13]. Recent studies have identified nonradiative recombination via defects between the perovskite and carrier transport layer interfaces as a major source of efficiency loss in perovskite solar cells [14–17]. Both of theory and experiment prove uncoordinated Pb^{2+} and/or halide (Cl^-, Br^-, I^-) ions as the dominant recombination defects, which reduces the fill factor (FF), open circuit voltage (V_{oc}) and overall device performance. Furthermore, for large area perovskite solar cells (>1 cm^2) because of the approximately linear increase in series resistance, it is always difficult to get a better fill factor than in small area solar cells [18]. To bridge the gap between the Shockley–Queisser efficiency limit and experimental PCE values, it is imperative to minimize the sources of recombination between perovskite films and charge transport layer (CTL) interfaces.

To overcome the problems of carrier recombination in perovskite solar cells, Huang et al. proposed an insulating polystyrene (PS) tunneling layer between the perovskite and electron transport layer (ETL) interface for inverted PSCs [19,20]. The thin insulating layer allows the transport of photogenerated electrons to ETL by tunnelling and blocks the photogenerated holes going through the ETL because of energy-mismatching in C_{60} for holes, which thus suppresses the charge recombination at the perovskite/ETL interface. Stolterfoht et al. found that inserting ultrathin LiF (0.6–1 nm) interlayers between the perovskite and charge transport layers leads to substantial reduction of these interfacial losses, which results in significant enhancement of V_{oc} and FF [17]. White et al. proposed that inserting ultrathin PMMA films at both the perovskite/ETL and perovskite/hole transport layers (HTL) interfaces symmetrically reduces interface recombination [21–23]. The further design and selection of more excellent interlayer materials and the exploration of their different functions are particularly important for

* Corresponding author. Key Laboratory for Physical Electronics and Devices of the Ministry of Education & Shaanxi Key Lab of Information Photonic Technique, School of Electronic and Information Engineering, Xi'an Jiaotong University, No. 28, Xianning West Road, Xi'an, 710049, China.
E-mail address: zhaoxinwu@mail.xjtu.edu.cn (Z. Wu).

https://doi.org/10.1016/j.orgel.2020.105937
Received 23 July 2020; Received in revised form 25 August 2020; Accepted 27 August 2020
Available online 22 September 2020

the preparation of large-area devices.

In this work, we propose a serial of alkali metal fluorides as functional interlayers at the perovskite/ETL interface by vapor deposition method. The alkali metal fluorides layer can function as both passivation layer and physical barrier layer. The bifunctional layer significantly improves the efficiency and stability of PSCs, especially improving the fill factor in large area perovskite solar cells with optimal KF interlayer, which is key to achieve high efficiency large area solar cells. Eventually, we achieve the best fill factor (80.6%) for 1 cm^2 size and highest FF (73.1%) for 10.8 cm^2 size perovskite solar cells with KF interlayer. This new ultra-thin inorganic interlayer strategy is a promising method for achieving industrial fabrication requirements with high fill factor, low cost and high efficient large area planar perovskite solar cells.

2. Experimental

2.1. Materials

Methylammonium iodide (MAI) was synthesized according to a previous study [22], in brief: 24 mL methylamine solution (33 wt% in ethanol, Sigma Aldrich) and 10 mL hydriodic acid (57 wt% in water, Sigma Aldrich) were diluted by 100 mL ethanol in a 250 mL round bottom flask by constant stirring at 0 °C for 2 h. The precipitate of CH_3NH_3I was gained by rotary evaporation at 40 °C and washed with dry diethyl ether until the solid became white. The final product was dried at 60 °C in a vacuum oven for 24 h. PbI_2 (99.999 wt%) was purchased from Alfa Aesar. PEDOT:PSS (CLEVIOS PH 1000) solution was acquired from Haraeus and used as received. Alkali metal fluorides (AF, 99.5 wt%) were purchased from J&K Chemical without further purification. C_{60} (99%) and BCP (99%) were purchased from Nichem (Taiwan).

2.2. Device fabrication

The cleaning process of the ITO-coated glass (12 Ω/sq) could be found in our previous report [23]. PEDOT:PSS/deionized water (v/v = 1/3) solutions by sonication and filtering were first spin-coated onto the substrate at 1500 rpm for 30 s and annealed 20 min at 130 °C. The $MAPbI_3$ perovskite film was deposited using a two-step evaporation-spin coating method following our previous work [22]. We transferred the ITO substrates coated with PEDOT:PSS to a vacuum chamber. The PbI_2 films of 200 nm thickness were sublimated under a pressure of 10^{-5} mbar at a rate of 8.0 Å/s and the resulting substrates were placed into a N_2-filled glovebox heated for 5 min at 50 °C; The CH_3NH_3I solution (80 mg/mL in 2-propanol) was dropped on the ITO/PEDOT:PSS/PbI_2 substrates, then the annealing for 2 h at 50 °C. After annealing, alkali metal fluorides materials with thickness of 3 nm were deposited on top of perovskite at the rate of 0.2 Å/s by vacuum evaporation. Eventually, the devices were completed by consecutively vacuum depositing C_{60} (30 nm), BCP (6 nm) and Ag cathode (120 nm) under 1×10^{-5} mbar at a rate of 0.3 Å/s, 0.3 Å/s and 1.0 Å/s, respectively. The complete device structure can be formed with ITO/PEDOT:PSS/$MAPbI_3$/AF/C_{60}/BCP/Ag. The 1 cm^2 and 10.8 cm^2 large area perovskite solar cell followed the same procedures.

2.3. Characterization

All measurements were conducted in ambient air. The photovoltaic performance was evaluated under an AAA solar simulator (XES-301S, SAN-EI), AM 1.5G irradiation with an intensity of 100 mW/cm^2. The photocurrent–voltage (J–V) curves were measured by a Keithley 2602 source meter under simulated sunlight and the scan rate was 0.5 V s^{-1} starting from −0.05 to 1.2 V. The absorption spectra were acquired on a UV–Vis spectrophotometer (HITACHI U-3010, Japan). The PL lifetime was recorded in a FLS 920 Fluorescence Lifetime and Steady State Spectroscopy (Edinburgh Instruments, British). The morphology and crystallinity were investigated by scanning electron microscopy (SEM) (Quanta 250, FEI). The crystalline structures on ITO substrate were performed with an X-ray diffractometer (D/MAX-2400, Rigaku, Japan) with Cu K_α radiation ($\lambda = 0.154060$ nm). Electrochemical impedance spectroscopy with the range of 0.1 Hz–1 MHz was performed by electrochemical workstation (CHI600E, CH Instruments, China) at the bias of the respective open-circuit voltage.

3. Results and discussion

The method of two-step evaporation-spin coating is illustrated in Fig. 1a. Firstly, the PbI_2 films of 200 nm are sublimated under a pressure of 10^{-5} mbar at a rate of 8.0 Å/s, and then the CH_3NH_3I solution (80 mg/mL in 2-propanol) is dropped on the ITO/PEDOT:PSS/PbI_2 substrates. Subsequently, the annealing is performed under a nitrogen atmosphere for 2 h at 50 °C. After annealing, alkali metal fluorides materials with thickness of 3 nm were deposited on top of perovskite at the rate of 0.2 Å/s by vacuum evaporation. In order to explore the effect of alkali metal fluoride, firstly, we carry out the SEM measurement as shown in Fig. 1b. The surface SEM images for perovskite absorbers with different alkali metal fluorides layer indicate similar morphology. However, the alkali metal fluoride is too thin to be seen clearly. Atomic force microscope (AFM) images (Fig. S1) were used to study the roughness of the obtained films. The root mean square (RMS) roughness of pristine perovskite is 13.06 nm, and it increases to 16.26 nm, 17.75 nm after vapor evaporation an ultra-thin CsF, RbF interlayer, respectively. Interestingly, it increases to 18.12 nm for KF interlayer. It is easy to understand that ultra-thin alkali metal fluoride slightly changes the surface roughness. The profile elemental (alkali cations and fluorine) mapping from the energy-dispersive X-ray (EDX) spectroscopy clearly indicate their homogeneous distribution on the perovskite interface as shown in Fig. S2.

X-ray diffraction (XRD) are carried out to investigate the crystallization of the $MAPbI_3$ films. Fig. S3 shows the X-ray diffraction (XRD) patterns for the perovskite films containing various alkali metal fluorides materials prepared on ITO/PEDOT:PSS substrates. Obviously, the typical diffraction peaks including (110), (220) are detected in all samples, which indicates the existence of the tetragonal phase of perovskite. The stronger diffraction peak with AF modified suggesting that the crystallinity and crystal orientation are improved. There is no obviously diffraction peak shift in all films, which reveal that alkali metal fluorides may only modify the perovskite interface.

In order to further verify the optical properties by alkali metal fluorides, we measured the absorption spectrum and photoluminescence (PL) of perovskites with different alkali metal fluorides. Fig. 2a shows the optical absorption spectra of perovskite films containing various alkali metal fluorides fabricated on glass substrates. The perovskite containing KF shows a red shift in the absorption edge. Oppositely, the perovskites containing RbF or CsF present blue shift in the absorption edge. To quantitatively assess the influence of the alkali metal fluorides interlayer on the band gap of perovskite materials, the band gaps are calculated according to Tauc plot, as illustrated in Fig. 2b [24]. The detailed calculations results of Tauc plot are shown in Table S1. The band gap is 1.612 eV for perovskites containing KF, suggesting a shrinkage compared to the pristine perovskites (1.614 eV). However, the RbF (1.617 eV) and CsF (1.629 eV) give rise to an extension of the band gap.

Simultaneously, the photoluminescence (PL) spectra and corresponding decay curves are measured for the perovskite films containing various alkali metal fluorides. To avoid the influence of hole injection to PEDOT:PSS during evaluating the lifetime, the perovskite films are deposited on glass substrates. Fig. S4 shows the related PL spectra, indicating that the intensity dramatically enhances with alkali metal fluorides. Fig. 2c and d show the related normalized PL spectra and decay curves. It is clear that the PL peaks slightly shift towards long wavelength after KF interlayer modified. The RbF and CsF containing perovskite films show blue shift compared to the pristine perovskite.

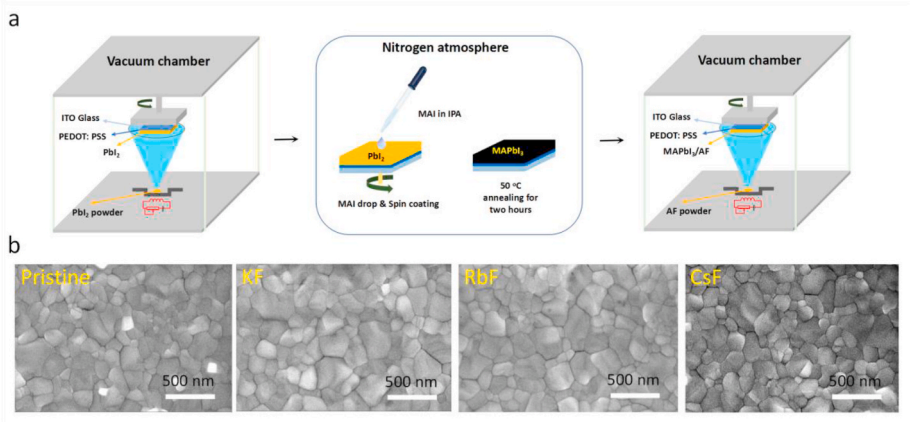

Fig. 1. (a) Schematic of two-step evaporation-spin coating method and vapor evaporation alkli metal flourides (AF, A = K, Rb, Cs). (b) SEM images for perovskite films without and with AF.

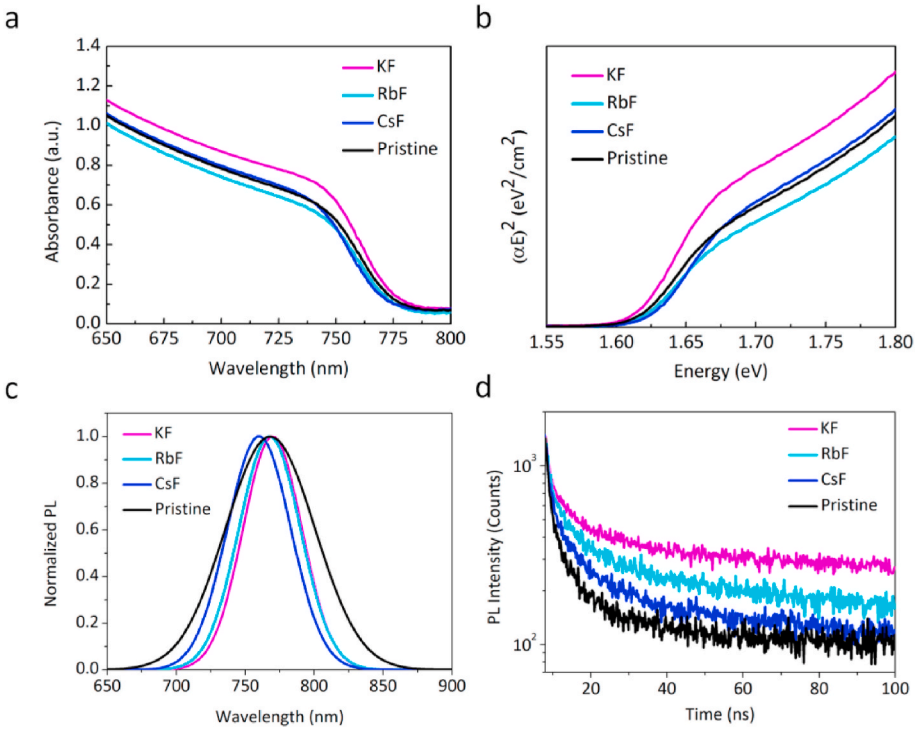

Fig. 2. (a) Absorbance spectra (b) Band gap (c) PL spectra and (d) PL decay curves for perovskite films without and with various alkali metal fluorides.

This result is consistent with the absorption spectra, and further evidencing the variation of band gap after alkali metal fluorides modified. The corresponding decay curves, fitted by bi-exponential function as shown in Table S2, indicated that the modification with RbF and CsF enhance the carrier lifetime. Meanwhile, the KF containing perovskite presents the longest carrier lifetime. This result suggests that the modification of alkali metal cations improve the carrier lifetime and therefore high photovoltaic performance is expected.

The perovskite solar cells with the structure of ITO/PEDOT:PSS/$MAPbI_3$/Alkali Metal Fluorides (AF)/C_{60}/BCP/Ag are fabricated, the relevant cross-section SEM as shown in Fig. 3a. The detailed preparing processes are stated in the experimental sections. Fig. S5 shows the energy level alignment of the planar PSC with and without alkali metal fluorides. Energy level changes related to the photovoltaic performance [25–27], therefore, the devices structure with alkali metal fluorides modified eventually improve the photoelectric properties. Changing the thickness of the alkali fluorides (Fig. S6), the optimal value confirmed is 3 nm by comparing the power conversion efficiency of devices. Fig. 3b present the dependence of the photovoltaic parameters of the devices on the various alkali metal fluorides. As can be seen, the average PCE increases with the alkali metal fluorides, owing to the significantly improved FF, J_{sc} and slightly enhanced V_{oc}.

The representative *J-V* curves is shown in Fig. 3c. It is found that alkali metal fluorides can enhance the PCE of perovskite solar cells and the devices obtaining KF interlayer have the highest PCE 16.21% with a V_{oc} as high as 0.87 V, a J_{sc} of 24.11 mA/cm^2 and an FF of 0.821. The detailed photovoltaic parameters with different alkali metal fluorides were summarized in Table S3. These results are consistent with other literatures, where photovoltaic performance increased after the K^+, Rb^+ or Cs^+ incorporation owing to the defect passivation, larger grain [28–31]. The values of integrated current density deduced from the incident photon to current conversion efficiency (IPCE) measurements are 22.54 mA/cm^2, 21.44 mA/cm^2, 20.52 mA/cm^2, and 19.50 mA/cm^2, which is in agreement with the value from the *J-V* scanning. Because of

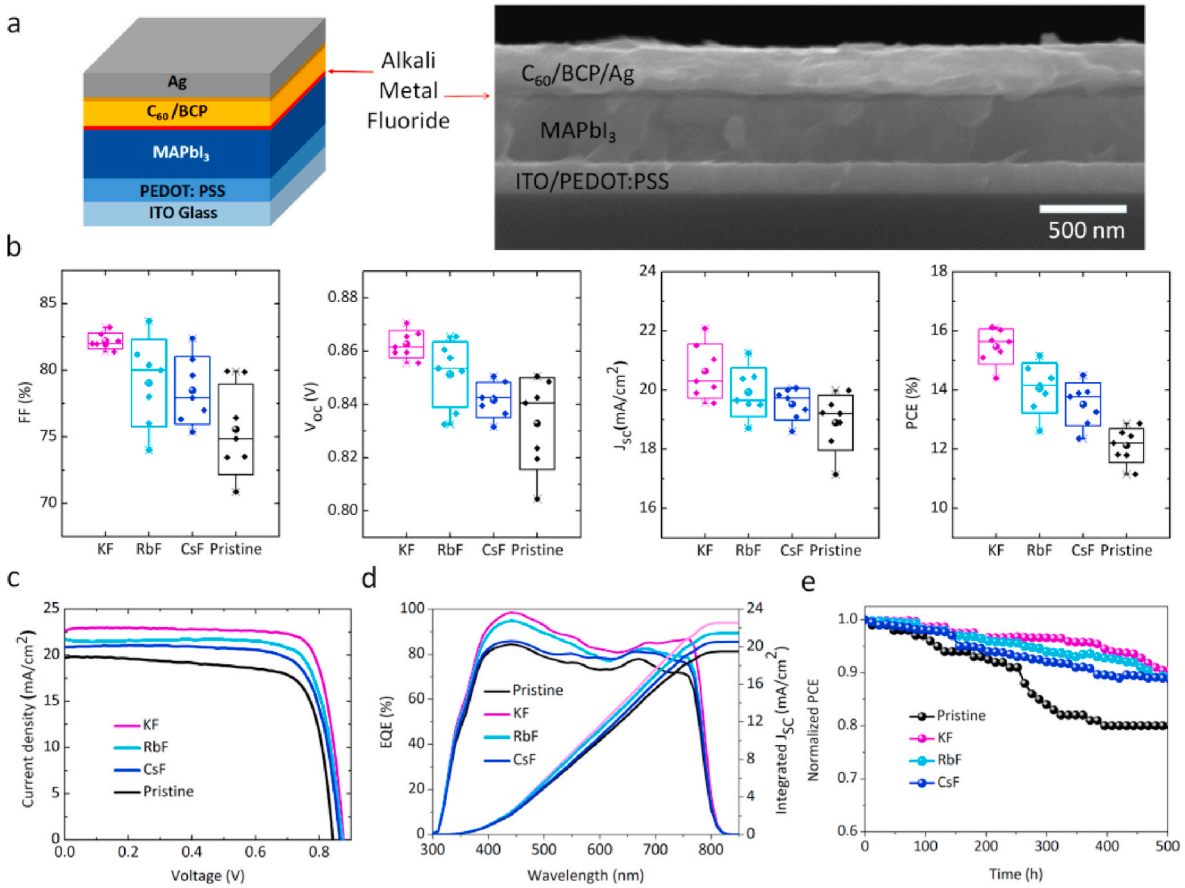

Fig. 3. (a) Schematic diagram of solar cell configuration and cross-sectional SEM image in inverted perovskite solar cells deposited with different alkali metal fluorides (scale bar: 500 nm). Pristine and different alkali metal fluoride modified devices: (b) Statistic photovoltaic parameters obtained FF, V_{oc}, J_{sc}, and PCE. (c) *J-V* curves of representative devices, (d) IPCE and integrated current density, (e) Stability of devices by exposing them to air (40% RH) for 500 h without encapsulation.

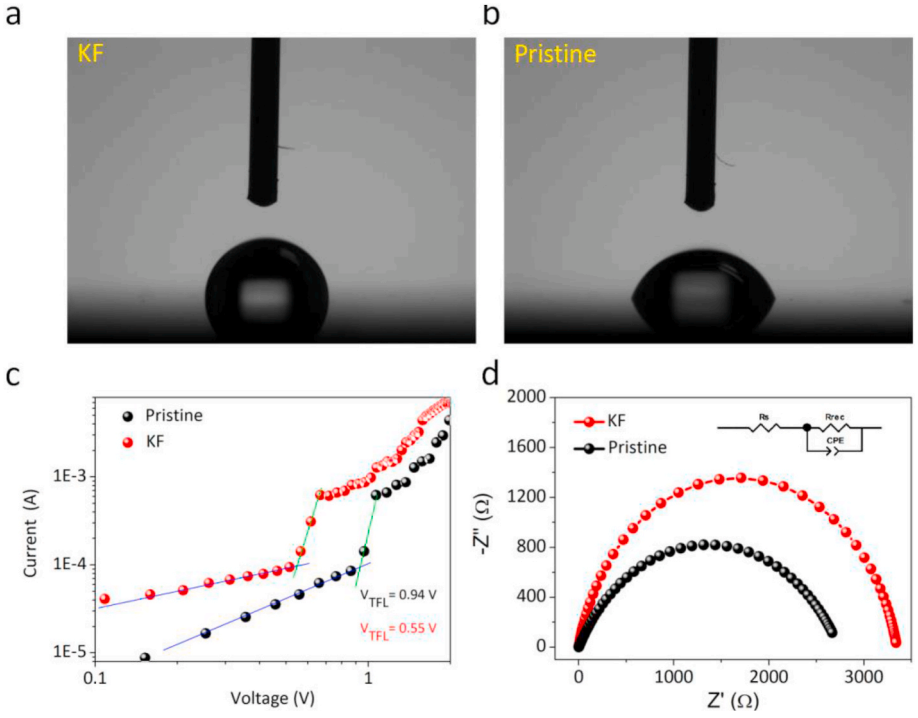

Fig. 4. (a) The contact angle for perovskite films without and with KF. Current–voltage (I–V) characteristics of (b) electron-only devices. (c) EIS of PSCs for pristine and KF modified.

no obvious difference in the absorption spectra, the J_{SC} increase can be explained by the reduced traps from the interface.

Finally, the stabilities of the $MAPbI_3$ without and with AF modified are also studied by exposing them to air (40% RH) for 500 h without encapsulation. Fig. 3e depicts the normalized PCE change of the different devices. Compared with the pristine $MAPbI_3$ device of 20% attenuation efficiency, the device modified with KF shows excellent stability with an efficiency attenuation of 10%.

Subsequently, we tested the contact angle, the space-charge-limited-current (SCLC) and electrochemical impedance spectroscopy (EIS) for films and devices to confirm the reasons improvement of the stability and efficiency, and especially represented by KF.

As displayed in Fig. 4a and b, the angle of pristine film is 68.95°, the value obviously increase to 89.13°, indicating a significant improving of hydrophobic after modification, similar phenomenon happening on the RbF and CsF intelayer modified (Fig. S7), detailed date as shown in Table S4. The bigger surface hydrophobic contribute to the stability, which shows the unique advantages for inorganic interlayer applied at interface.

SCLC tests in dark conditions assess the intrinsic characteristics of perovskite films. The single electronic devices construct with the structure of ITO/C_{60}/perovskite/with or without AF/C_{60}/Ag. In Fig. 4c, the voltage of trap filling limit (V_{TFL}) of pristine $MAPbI_3$ films is 0.94 V, and the trap state density is calculated to be 1.81×10^{16} cm^{-3}, according to the formula in Supporting information. While the values with KF interlayer modified drops to 0.55 V, and the corresponding density of the trap state is 1.06×10^{16} cm^{-3}. These results reflect that the KF interlayer can effectively reduce the defects states density of perovskite/ELT interface, contributing the improvement of FF.

To gain deep insight into the alkali metal fluorides-induced enhancement of power conversion efficiency, we take the electrochemical impedance spectroscopy (EIS) measurement, a useful technique that reveals the potential carrier transport behaviors in the PSCs. The Nyquist plots of these devices with alkali metal fluorides or without were obtained with an applied bias voltage of 0.8 V close to the V_{oc} as shown in Fig. 4d. Then the EIS data obviously shows the improved recombination resistance in PSCs with the KF layer has the large recombination resistance which is consistent with the high PCE attained using KF layer as shown in Fig. 3c. Larger recombination resistance R_{rec} for free carriers indicates less carrier recombination probability and thereby reduced charge loss in the photocurrent. As a result, higher V_{oc}, J_{sc}, and FF are realized in the device using KF. According to the above analysis, perovskite solar cell modified with the alkali metal fluorides, which can reduce the trap state density and increase the recombination resistance, suppress the nonradiative recombination at interfaces, directly resulting in high fill factor in devices.

To confirm the benefits of the inserting an alkali metal fluorides layer, the complete perovskite solar cell devices with structure glass/ITO/PEDOT:PSS/$MAPbI_3$/KF/C_{60}/BCP/Ag were fabricated on substrates as shown in Fig. 5a (active area is 1 cm^2). The current density-voltage (*J-V*) characteristics of the cell is shown in Fig. 5b. The fill factor reaches up to 80.6% when the active area is 1 cm^2. To the best of our knowledge, we have achieved the high fill factor for 1 cm^2 size perovskite solar cell. Ultimately, we fabricated a PSC module based on the this device structure. As shown in Fig. 5c and Fig. S8, the PSC module with an effective area of 10.8 cm^2 consists of eight sub-PSCs with an effective area of 1.35 cm^2 (0.30 cm × 4.5 cm). The sub-PSCs are connected in series by effectively masking each functional layer and the distance between adjacent sub-PSCs is 5.6 cm. Fig. 5d shows the best performance of the champion module with a PCE of 10.24%, a V_{oc} of 6.83V, a J_{sc} of 2.05 mA/cm^2 and an FF of 73.1% under reverse scanning.

The proposed alkali metal fluorides functional layer at the perovskite/ETL interface by vapor deposition method can significantly improve the efficiency of PSCs, especially for the improving of the FF in large area perovskite solar cells, which is indispensable for high efficiency large area solar cells. We are also experimenting with module to drive low-power devices as shown in Fig. S9. Fig. S10 depicts the normalized PCE of the devices for 21 consecutive days. Compared with the $MAPbI_3$ device of 42% attenuation efficiency, the KF modified device shows excellent stability with an efficiency attenuation of 17%.

4. Conclusion

In conclusion, we demonstrate that alkali metal fluorides interlayer

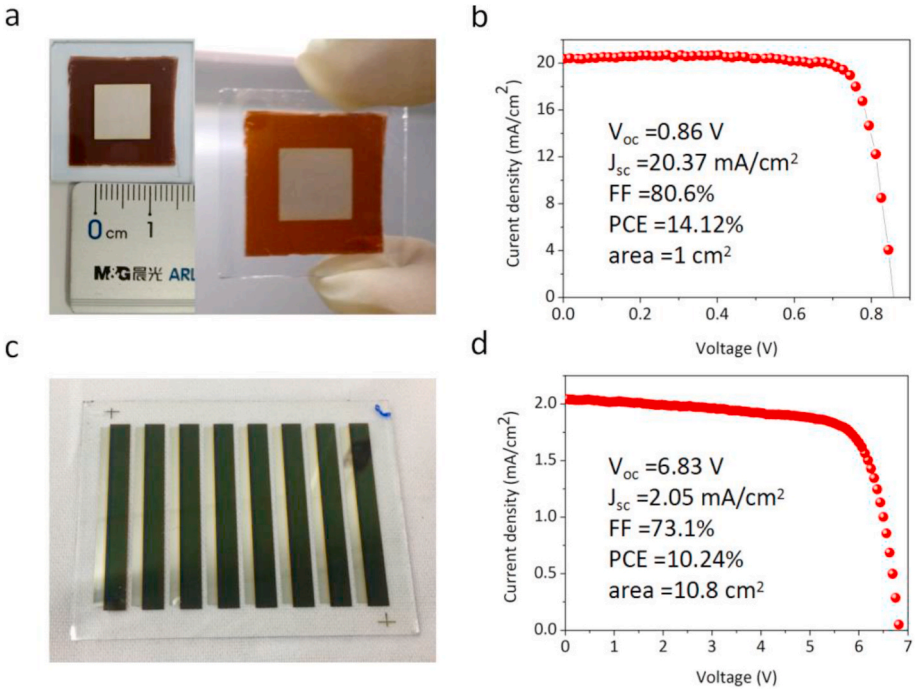

Fig. 5. (a) Image of device with 1 cm^2. (b) Current density–voltage (*J–V*) characteristics of 1 cm^2 perovskite cells with KF interlayer. (c) Image of $MAPbI_3$ module with an effective area of 10.8 cm^2 (8 sub-cells in series). (d) Current density–voltage (*J–V*) characteristics of 10.8 cm^2 perovskite cells with KF interlayer.

between perovskite and ETL could significantly increase device performance functioning as suppressing carrier recombination by passivating the perovskite/ETL interface. The ultrathin inorganic interlayer can significantly improve the efficiency of PSCs, especially for improving the fill factor in large area perovskite solar cells, which is indispensable for high efficiency large area solar cells. In this paper, we achieve the best fill factor (80.6%) for 1 cm^2 size and highest FF (73.1%) for 10.8 cm^2 size perovskite solar cells. This functional interlayer strategy paves the way to resolve the industrial requirements with low cost, high fill factor large area planar perovskite solar cells.

Declaration of competing interest

The authors declare that they have no known competing financial interests or personal relationships that could have appeared to influence the work reported in this paper.

Acknowledgements

This work is financially supported by National Natural Science Foundation of China (Grant Nos. 11574248, 61505161). China Postdoctoral Science Foundation (Grant No. 2019M663717), Scientific Research Plan Projects of Shaanxi Education Department (Grant No.17JK0700), Natural Science Basic Research Plan in Shaanxi Province of China (Grant No. 2019JQ-119), The SEM work is performed at International Center by Dielectric Research (ICDR), Xi'an Jiaotong University, Xi'an, China.

Appendix A. Supplementary data

Supplementary data to this article can be found online at https://doi.org/10.1016/j.orgel.2020.105937.

References

[1] A. Kojima, K. Teshima, Y. Shirai, T. Miyasaka, Organometal halide perovskites as visible-light sensitizers for photovoltaic cells, J. Am. Chem. Soc. 131 (2009) 6050–6051.
[2] H.-S. Kim, C.-R. Lee, J.-H. Im, K.-B. Lee, T. Moehl, A. Marchioro, S.-J. Moon, R. H. Baker, J.- Yum, J.E. Moser, M. Grätzel, N.-G. Park, Lead iodide perovskite sensitized all-solid-state submicron thin film mesoscopic solar cell with efficiency exceeding 9%, Sci. Rep. 2 (2012) 591.
[3] J. Dai, J. Xi, Y. Zu, L. Li, J. Xu, Y. Shi, X. Liu, Q. Fan, J. Zhang, S. Wang, F. Yuan, H. Dong, B. Jiao, X. Hou, Z. Wu, Surface mediated ligands addressing bottleneck of room-temperature synthesized inorganic perovskite nanocrystals toward efficient light-emitting diodes, Nanomater. Energy 70 (2020) 104467.
[4] P. Li, H. Dong, J. Xu, J. Chen, B. Jiao, X. Hou, J. Li, Z. Wu, Ligand orientation-induced lattice robustness for highly effifffifficient and stable tin based perovskite solar cells, ACS Energy Lett 5 (2020) 2327–2334.
[5] W.S. Yang, B.-W. Park, E.H. Jung, N.J. Jeon, Y.C. Kim, D.U. Lee, S.S. Shin, J. Seo, E. K. Kim, J.H. Noh, S. Il Seok, Iodide management in formamidinium-lead-halide–based perovskite layers for efficient solar cells, Science 356 (2017) 1376.
[6] M.A. Green, Y. Hishikawa, E.D. Dunlop, D.H. Levi, J.H. Ebinger, M. Yoshita, A.W.Y. H. Baillie, Solar cell efficiency tables (Version 53), Prog. Photovoltaics Res. Appl. 27 (2019) 3–12.
[7] K. Yoshikawa, H. Kawasaki, W. Yoshida, T. Irie, K. Konishi, K. Nakano, T. Uto, D. Adachi, M. Kanematsu, H. Uzu, K. Yamamoto, Silicon heterojunction solar cell with interdigitated back contacts for a photoconversion efficiency over 26%, Nat. Energy 2 (2017) 17032.
[8] O. Yaffe, Y. Guo, L.Z. Tan, D.A. Egger, T. Hull, C.C. Stoumpos, F. Zheng, T.F. Heinz, L. Kronik, M.G. Kanatzidis, J.S. Owen, A.M. Rappe, M.A. Pimenta, L.E. Brus, Local polar fluctuations in lead halide perovskite crystals, Phys. Rev. Lett. 118 (2017) 136001.
[9] X. Wu, L. Tan, X. Shen, T. Hu, K. Miyata, M.T. Trinh, R. Li, R. Coffee, S. Liu, D. A. Egger, I. Makasyuk, Q. Zheng, A. Fry, J.S. Robinson, M.D. Smith, B. Guzelturk, H. I Karunadasa, X. Wang, X. Zhu, L. Kronik, A. M Rappe, A. M Lindenberg, Light-induced picosecond rotational disordering of the inorganic sublattice in hybrid perovskites, Sci. Adv. 3 (2017) 1602388.
[10] D.A. Egger, A.M. Rappe, L. Kronik, Hybrid organic–inorganic perovskites on the move, Chem. Res. 49 (2016) 573.
[11] D.A. Egger, A. Bera, D. Cahen, G. Hodes, T. Kirchartz, L. Kronik, R. Lovrincic, A. M. Rappe, D.R. Reichman, O. Yaffe, What remains unexplained about the properties of halide perovskites? Adv. Mater. 30 (2018) 1800691.
[12] G. Batignani, G. Fumero, A. Ram, S. Kandada, G. Cerullo, M. Gandini, C. Ferrante, A. Petrozza, T. Scopigno, Probing femtosecond lattice displacement upon photo-carrier generation in lead halide perovskite, Nat. Commun. 9 (2018) 1971.
[13] F. Ambrosio, J. Wiktor, F.D. Angelis, A. Pasquarello, Origin of low electron–hole recombination rate in metal halide perovskites, Energy Environ. Sci. 11 (2018) 101.
[14] P. Schulz, Interface design for metal halide perovskite solar cells, ACS Energy Lett 3 (2018) 1287.
[15] S.D. Stranks, Nonradiative losses in metal halide perovskites, ACS Energy Lett 2 (2017) 1515.
[16] J. Xu, H. Dong, J. Xi, Y. Yang, Y. Yu, L. Ma, J. Chen, B. Jiao, X. Hou, J. Li, Z. Wu, Local nearly non-strained perovskite lattice approaching a broad environmental stability window of efficient solar cells, Nanomater. Energy 75 (2020) 104940.
[17] M. Stolterfoht, C.M. Wolff, J.A. Márquez, S. Zhang, C.J. Hages, D. Rothhardt, S. Albrecht, P.L. Burn, P. Meredith, T. Unold, D. Neher, Visualization and suppression of interfacial recombination for high-efficiency large-area pin perovskite solar cells, Nat. Energy 3 (2018) 847.
[18] J. Kim, J.S. Yun, Y. Cho, D.S. Lee, B. Wilkinson, A. Ma Soufiani, X. Deng, Ji Zheng, A. Shi, S. Lim, S. Chen, Z. Hameiri, M. Zhang, C.F.J. Lau, S. Huang, M.A. Green, A. W.Y. Ho-Baillie, Overcoming the challenges of large-area high-efficiency perovskite solar cells, ACS Energy Lett 2 (2017) 1978.
[19] Q. Wang, Q. Dong, T. Li, A. Gruverman, J. Huang, Thin insulating tunneling contacts for efficient and water-resistant perovskite solar cells, Adv. Mater. 28 (2016) 6734.
[20] X. Wen, J. Wu, M. Ye, D. Gao, C. Lin, Interface engineering via an insulating polymer for highly efficient and environmentally stable perovskite solar cell, Chem. Commun. 52 (2016) 11355.
[21] J. Peng, J.I. Khan, W. Liu, E. Ugur, T. Duong, Y. Wu, H. Shen, K. Wang, H. Dang, E. Aydin, X. Yang, Y. Wan, K.J. Weber, K.R. Catchpole, F. Laquai, S.D. Wolf, T. P. White, A universal double-side passivation for high open-circuit voltage in perovskite solar cells: role of carbonyl groups in poly(methyl methacrylate), Adv. Energy Mater. 8 (2018) 1801208.
[22] J. Xi, Z. Wu, H. Dong, B. Xia, F. Yuan, B. Jiao, L. Xiao, Q. Gong, X. Hou, Controlled thickness and morphology for highly efficient inverted planar heterojunction perovskite solar cells, Nanoscale 7 (2015) 10699.
[23] H. Dong, J. Xi, L. Zuo, J. Li, Y. Yang, D. Wang, Y. Yu, L. Ma, C. Ran, W. Gao, B. Jiao, J. Xu, T. Lei, F. Wei, F. Yuan, L. Zhang, Y. Shi, X. Hou, Z. Wu, Conjugated Molecules"Bridge": functional ligand toward highly efficient and long-term stable perovskite solar cell, Advanced Functional Materals 29 (2019) 1808119.
[24] J. Tauc, R. Grigorovici, A. Vancu, Optical properties and electronic structure of amorphous germanium, Phys. Status Solidi B 15 (1966) 627.
[25] W. Zhang, X. Zhang, T. Wu, W. Sun, J. Wu, Z. Lan, Interface engineering with NiO nanocrystals for highly efficient and stable planar perovskite solar cells, Electrochim. Acta 293 (2019) 211.
[26] Y. Dou, D. Wang, G. Li, Y. Liao, W. Sun, J. Wu, Z. Lan, Toward highly reproducible, efficient, and stable perovskite solar cells via interface engineering with CoO nanoplates, ACS Appl. Mater. Interfaces 11 (2019) 32159.
[27] W. Zhang, J. Song, D. Wang, K. Deng, J. Wu, L. Zhang, Dual interfacial modification engineering with p-type NiO nanocrystals for preparing efficient planar perovskite solar cells, J. Mater. Chem. C 6 (2018) 13034.
[28] P. Zhao, W. Yin, M. Kim, M. Han, Y.J. Song, T.K. Ahn, H.S. Jung, Improved carriers injection capacity in perovskite solar cells by introducing A-site interstitial defects, J. Mater. Chem. 5 (2017) 7905.
[29] D.-Y. Son, S.-G. Kim, J.-Y. Seo, S.-H. Lee, H. Shin, D. Lee, N.-G. Park, Universal approach toward hysteresis-free perovskite solar cell via defect engineering, J. Am. Chem. Soc. 140 (2018) 1358.
[30] J.K. Nam, S.U. Chai, W. Cha, Y.J. Choi, W. Kim, M.S. Jung, J. Kwon, D. Kim, J. H. Park, Potassium incorporation for enhanced performance and stability of fully inorganic cesium lead halide perovskite solar cells, Nano Lett. 17 (2017) 2028.
[31] S. Bag, M.F. Durstock, Large perovskite grain growth in low-temperature solution-processed planar p-i-n solar cells by sodium addition, ACS Appl. Mater. Interfaces 8 (2016) 5053.